$Au_xPd_{(300-x)}$ Alloy Nanoparticles for the Oxygen Reduction Reaction in Alkaline Media

Jamie A. Trindell[+],[a, b] Zhiyao Duan[+],[a, b, c] Graeme Henkelman,*[a, b, c] and Richard M. Crooks*[a, b]

$Au_xPd_{(300-x)}$ nanoalloys were prepared using a dendrimer-templating method and their electrocatalytic efficiencies towards the oxygen reduction reaction (ORR) were analyzed in alkaline media. The composition-dependent PdO_x reduction potentials of the $Au_xPd_{(300-x)}$ nanoalloys were correlated to the oxygen-binding (O-binding) energy of the catalysts. Multiple PdO_x reduction peaks were present for the $Au_{150}Pd_{150}$ and $Au_{50}Pd_{250}$ catalysts. These peaks were assigned to the alloyed and bulk-like Pd active sites on the alloyed surface. The results described here are significant because modulation of the O-binding energies improved the ORR activity on the nanoalloys. Specifically, a linear trend in O-binding energies of $Au_xPd_{(300-x)}$ dendrimers (DENs) as a function of Pd composition resulted in a volcano-shaped trend in ORR activity. The optimal O-binding energy of $Au_{50}Pd_{250}$ resulted in an approximate 89 mV shift in PdO_x reduction relative to Pd_{300} and a shift of approximately 76 mV in ORR peak potential.

1. Introduction

In this report we demonstrate that the oxygen-binding (O-binding) strength of Pd can be systematically modulated by controlling the composition of $Au_xPd_{(300-x)}$ nanoalloys in the ~2 nm size range. This is significant because pure Pd nanoparticles (NPs) bind oxygen too strongly for maximum ORR activity. Notably, we find that multiple Pd-oxide (PdO_x) reduction peaks correlate to the O-binding strengths on $Au_xPd_{(300-x)}$ alloys and thus correlate to the overall ORR activity of the catalyst.

Electronic (or ligand) and ensemble (or geometric) effects are two major effects responsible for tuning the binding energies of O. Indeed, we have previously shown that electronic effects and surface ensembles provide synthetic and theoretical handles for understanding and improving the catalytic activity of nanoalloys. Electronic effects can shift the d-band center of the surface alloy and thus tune the binding energies of reaction intermediates. Ensembles refer to the smallest number of atoms required to form a catalytically active site. For example, a triatomic surface ensemble, or three atoms in a triangular arrangement on the surface of a nanoparticle (NP) catalyst, is required to bind and reduce oxygen. Therefore, adsorbate (e.g., O or OH) binding energies on different ensembles can be determined electrochemically and used to predict the overall ORR activity of an alloy.

In one specific case, our groups previously reported on RhAu nanoalloys for the ORR.[1] Density functional theory (DFT) calculations predicted that triatomic Rh_1Au_2 ensembles possessed the optimal O- and OH-binding energies to be highly active sites for the ORR. The number and type (i.e., composition) of surface ensembles present on a random nanoalloy can be experimentally modulated by exerting control over their size and composition. Significantly, in the present report, we were able to directly observe the O-binding energies of different $Au_xPd_{(3-x)}$ surface ensembles via PdO_x reduction potentials and correlate them to the ORR activity.

The correlation of PdO_x reduction potentials with the ORR activity of Pd has been previously reported for Au@Pd core@-shell NPs. Specifically, Huang et al. deposited submonolayer amounts of Pd onto 9 nm Au cores.[2] The PdO_x reduction potential was then related to the surface coverage of Pd. When 90% of the Au core was covered with a monolayer of Pd, a ~240 mV shift in the PdO_x reduction potential was observed and the onset of ORR activity was improved by ~50 mV. In a study by Wang et al., a shift in the PdO_x reduction potential of ~11 nm AuCu@Pd NPs was correlated to ORR activity.[3] The intermetallic AuCu core induced strain in the Pd shell that weakened the O-binding energy, thereby shifting the PdO_x reduction potential positive by ~118 mV relative to pure Pd and increasing the specific ORR activity by ~5.4 times.

In contrast to Au@Pd NPs, AuPd alloys possess different Pd-based surface ensembles having unique O-binding energies. To study these ensemble effects, we prepared $Au_xPd_{(300-x)}$ nanoalloys using a dendrimer templating method.[4–6] Five catalysts, Au_{300}, $Au_{250}Pd_{50}$, $Au_{150}Pd_{150}$, $Au_{50}Pd_{250}$, and Pd_{300}, were synthesized and analyzed using cyclic voltammetry (CV) in

[a] Dr. J. A. Trindell,[+] Dr. Z. Duan,[+] Prof. G. Henkelman, Prof. R. M. Crooks
Department of Chemistry
The University of Texas at Austin
105 E. 24th Street, Stop A5300, Austin, Texas 78712-1224, USA
E-mail: henkelman@utexas.edu
crooks@cm.utexas.edu
[b] Dr. J. A. Trindell,[+] Dr. Z. Duan,[+] Prof. G. Henkelman, Prof. R. M. Crooks
Texas Materials Institute
The University of Texas at Austin
105 E. 24th Street, Stop A5300, Austin, Texas 78712-1224, USA
[c] Dr. Z. Duan,[+] Prof. G. Henkelman
Oden Institute for Computational Engineering and Science
The University of Texas at Austin
105 E. 24th Street, Stop A5300, Austin, Texas 78712-1224, USA
[+] These authors contributed equally to this work.

Supporting information for this article is available on the WWW under https://doi.org/10.1002/celc.202000971

0.10 M $HClO_4$. Importantly, two PdO_x reduction peaks were observed for the $Au_{150}Pd_{150}$ and $Au_{50}Pd_{250}$ nanoalloys. The potential of these PdO_x reduction peaks correlate to distinct O-binding energies on the triatomic surface ensembles Au_1Pd_2 and Pd_3. Specifically, a ~132 mV shift in PdO_x reduction potential, relative to pure Pd, was observed for $Au_{50}Pd_{250}$ nanoalloys. Theoretical calculations suggest that this potential shift results from the weakened O-binding strength of Au_1Pd_2 surface ensembles. Accordingly, the peak ORR potential of $Au_{50}Pd_{250}$ was positively shifted by ~76 mV relative to Pd_{300}.

Experimental Section

Chemicals

All chemicals were used as received unless otherwise noted. Sixth-generation, hydroxyl-terminated poly(amidoamine) dendrimers (G6OH) were purchased from Dendritech, Inc. (Midland, MI). Dendrimers were received as 10–25% solutions in methanol and dried under vacuum prior to use. Nafion 117 solution (5 wt% in methanol), $HAuCl_4 \cdot 3H_2O$ (≥99.9% trace metal grade), K_2PdCl_4 (98%), and $NaBH_4$ (99.99%) were purchased from Millipore-Sigma (St. Louis, MO). 2-propanol (Certified ACS Plus) was purchased from Fisher Scientific (Fair Lawn, NJ). Vulcan carbon (XC-72R), used to prepare the catalyst inks, was from Fuel Cell Store (College Station, TX). Gases, including O_2 (99.999%, research grade) and Ar (99.99%), were purchased from Praxair, Inc. (Austin, TX). $HClO_4$ (70%) was purchased from VWR Chemicals (Radnor, PA). Glassy carbon electrodes (GCEs) were polished using 0.3 μm alumina (Baikowski International Corporation, Charlotte, NC) and then 0.05 μm alumina (Buehler, Lake Bluff, IL). After polishing, GCEs were cleaned electrochemically in 0.10 M $HClO_4$. All aqueous solutions were prepared using deionized (DI) water (18.2 MΩ cm Milli-Q water, Millipore, Bedford, MA).

Synthesis of G6OH($Au_xPd_{(300-x)}$) DENs

To be clear, the notation G6OH($Au_xPd_{(300-x)}$) refers to the ratio of total metal ions (Au + Pd = 300) to the number of G6OH dendrimers used for the synthesis. It is not intended to suggest that every NP of a particular average composition has exactly the indicated stoichiometry (though previous studies indicate a close correspondence between the ratio of ions used in the synthesis and the final NPs).[7,8] All syntheses were conducted in an ice bath (~10 °C) under an Ar-saturated atmosphere. Using the synthesis of G6OH($Au_{150}Pd_{150}$) DENs as an example, first, 200.0 μL of a 100 μM G6OH poly(amidoamine) (PAMAM) dendrimer stock ($2.0 \cdot 10^{-8}$ mol G6OH PAMAM) were added to 8.30 mL of DI water with vigorous stirring. Second, 150.0 μL of a 20.0 mM K_2PdCl_4 stock solution ($3.0 \cdot 10^{-6}$ mol Pd^{2+}) was added drop-wise to the stirred G6OH solution. The Pd^{2+} precursor was allowed to complex within the dendrimer for 20 min. Third, 150.0 μL of 20.0 mM $HAuCl_4 \cdot 3H_2O$ ($3.0 \cdot 10^{-6}$ mol Au^{3+}) was added to the reaction solution drop-wise and with continued stirring. Fourth, the Pd^{2+}/Au^{3+}/G6OH complex was reduced with 1.20 mL of 0.10 M $NaBH_4$ (~67-fold molar excess relative to the metal precursors) ~2 min after the first addition of Au salt. Finally, the reaction mixture was removed from the ice bath and stirred at room temperature for 12 h to allow for deactivation of excess $NaBH_4$. The final reaction solution contained 10.0 mL of 2.0 μM G6OH($Au_{150}Pd_{150}$) DENs. For the other compositions of G6OH($Au_xPd_{(300-x)}$) DENs, the same procedure was used except that the ratio of Au:Pd was modified appropriately while keeping the total metal ion concentration constant.

The G6OH($Au_xPd_{(300-x)}$) DENs were immobilized on carbon as follows: 2.0 mL of the 2.0 μM G6OH($Au_xPd_{(300-x)}$) DENs solution, 200.0 μL isopropyl alcohol, 10.0 μL of 5.0 wt% Nafion 117 (in MeOH), and 2.0 mg of Vulcan carbon (C) were sonicated together for ~15 min. This resulted in an G6OH($Au_xPd_{(300-x)}$)/C conductive ink for use in electrochemical studies.

Electron Microscopy Characterization of G6OH($Au_xPd_{(300-x)}$) DENs

Size analysis of the as-synthesized G6OH($Au_xPd_{(300-x)}$) DENs was conducted using a JEOL 2010F transmission electron microscope (TEM) with a point resolution of 0.19 nm at an accelerating voltage of 200 kV. Samples were prepared by drop-casting 2.0 μL of 2.0 μM G6OH($Au_xPd_{(300-x)}$) DENs solution on copper-backed, 300 mesh, continuous-carbon grids (Electron Microscopy Sciences, Hatfield, PA). Size distributions were obtained by analyzing 200 particles from each sample using ImageJ. Scanning transmission electron microscopy and energy dispersive X-ray spectroscopy (STEM-EDX) of the G6OH($Au_xPd_{(300-x)}$)/C composite inks on lacey-carbon grids (Electron Microscopy Sciences, Hatfield, PA) were conducted using a JEOL NeoArm aberration-corrected TEM at an accelerating voltage of 80 kV and a resolution of 0.11 nm.

Electrochemical Measurements

All electrochemical measurements were obtained using a CH Instruments Model CHI700D Electrochemical Analyzer (Austin, TX) and a single-compartment, three-electrode electrochemical cell. Electrochemical potentials were measured vs. either a Hg/HgO/1.0 M NaOH or Hg/Hg_2SO_4/saturated K_2SO_4 reference electrode (CH Instruments, Inc.). All potentials reported herein were converted to the reversible hydrogen electrode (RHE) potential using the equation $E_{RHE} = E_{ref} + E^{\circ}_{ref} + 0.059$ pH, where E_{RHE} is the calculated potential vs. RHE and E_{ref} and E°_{ref} are the measured and standard potentials of the Hg/HgO/1.0 M NaOH or Hg/Hg_2SO_4/saturated K_2SO_4 reference electrodes, respectively. A glassy carbon rod (100 mm long, 6 mm in diameter, Alfa Aesar, Tewksbury, MA) was used as the counter electrode. Catalyst-coated working electrodes were prepared by drop casting 6.0 μL of $Au_xPd_{(300-x)}$/C ink onto a 3 mm glassy carbon disk electrode and then drying the ink under a gentle flow of Ar. Between each set of electrochemical experiments, the working electrode was polished using 0.05 μm alumina (Buehler, Lake Bluff, IL).

The electrocatalysis measurements were carried out as follows. First, the catalysts were electrochemically cleaned via cyclic voltammetry (CV) in Ar-saturated, 0.10 M $HClO_4$ (pH = 1.0). Specifically, the catalysts were cycled 20 times between 0.05 V and 1.57 V at 200 mV/s, at which point the CVs attained limiting behavior. After electrochemical cleaning, three CVs were collected at 50 mV/s in the same potential range used for the cleaning cycles. The final CV was used to analyze the AuO_x and PdO_x reduction peak potentials of each catalyst. The charge under the AuO_x and PdO_x reduction peaks was used to calculate the electrochemically active surface areas (ECSA) of Au and Pd using the conversion factors of 390 μC/cm^2 and 424 μC/cm^2, respectively.[3,9,10] These initial ECSA values were used to calculate current densities.

Second, the electrocatalytic ORR activities of the catalysts were analyzed in O_2-saturated, 0.10 M KOH (pH = 13.0). The potentials used for collecting ORR CVs was dependent on the particular catalyst under study, but it ranged between 0.95 V and 0.55 V. Five CVs were collected at which point limiting behavior was attained. Accordingly, the fifth ORR CV for each catalyst was used for analysis.

Electrochemical surface characterization after ORR experiments was carried out by obtaining three additional CVs between 0.05 V and 1.57 V at 50 mV/s in Ar-saturated, 0.10 M $HClO_4$ (pH = 1.0). The ECSAs obtained from the third CV were compared to the ECSA obtained prior to the ORR to assess the stability of the catalyst under electrocatalytic conditions.

Density Functional Theory

Plane-wave-based density functional theory (DFT) calculations were performed using the Vienna ab initio simulation package.[11–13] The exchange correlation energy was described within the generalized gradient approximation using the Perdew-Burke-Ernzerhof functional.[14] The interaction between the valence and core electrons was treated within the projected augmented wave framework.[15] Kohn-Sham orbitals were expanded in a plane-wave basis with a kinetic energy cut-off of 400 eV. The Brillouin zone was sampled by a 4×4×1 grid of *k* points following the Monkhorst-Pack scheme.[16] A threshold of 10^{-5} eV was used for the convergence of the electronic structure. Optimized structures were obtained by minimizing the forces on each ion until they fell below 0.01 eV/Å. Metal surfaces were modeled with four-layer slabs separated by 12 Å of vacuum. The top two layers were allowed to relax, and the bottom two layers were kept fixed at the bulk positions. The supercell in the xy-plane had a geometry of $4\times2\sqrt{3}$ R90°, which contains 16 metal atoms in each layer of the slab model.

Oxygen Binding Energy Calculations

We computed the O binding energy as a function of O* coverage and alloy composition. The atomic models of the alloy surfaces had 25, 50, and 75 at.% of Au randomly distributed in the Pd host. It should be noted that the Au composition in each layer was made equal to the overall composition. The atomic models of the alloy surfaces had the same supercell configuration as the pure metal surfaces described in the previous section, while the lattice constants were scaled to the weighted average of pure Pd and Au according to the alloy compositions.

On these alloy surfaces, O binding energies were computed as a function of O* coverage. Five O coverages were examined for each alloy surface: 1/16, 1/8, 3/16, 1/4, 5/16, 3/8, 7/16, and 1/2 of a monolayer. The optimal arrangement of O* was determined using the basin hopping algorithm.[17] In these calculations, we prescribed 96 adsorption sites for O*: 16 atop sites, 48 bridge sites, and 32 3-fold hollow sites. Initially, the O* were distributed randomly on the surface. Trial structures were generated by moving one randomly selected O* to another random adsorption site. A successful trial move avoids close proximity (within a radius distance of 2 Å) of other O* species. Each trial move was followed by structural relaxation. The decision to accept or reject of a trial structure was determined by the Metropolis algorithm.[18] For each basin hopping simulation, 200 trial structures were generated, and the structure with the lowest energy was used to calculate the O binding energy. For each Au composition, three slab models having different Au distributions were used to obtain average O binding energies and standard deviations due to the random Au distributions. Thus, for each O binding energy at a particular Au composition and O* coverage, 600 DFT calculations were performed. Each O binding energy was calculated as $\Delta E_O = (E_{nO/slab} - E_{slab} - E_{H2O} + E_{H2})/n$. We also calculated the differential binding, $\Delta E_O = (E_{nO/slab} - E_{(n-1)O/slab} - E_{H2O} + E_{H2})$, which describes the adsorption energy of each subsequently deposited O on the surface.

Computational Hydrogen Electrode Method

The thermochemistry of the electrochemical ORR was calculated by applying the computational hydrogen electrode method.[19] Briefly, the Gibbs free energy change of each elementary electrochemical step of the ORR and was calculated using DFT. The ORR reaction mechanism was assumed to follow the dissociative mechanism represented in Equations (1)–(3).

$$^1/_2\ O_2 + * \leftrightarrow O^* \quad (1)$$

$$O^* + H^+ + e^- \leftrightarrow OH^* \quad (2)$$

$$OH^* + H^+ + e^- \leftrightarrow H_2O + * \quad (3)$$

The free energy change of each elementary steps can be calculated as $\Delta G = \Delta E - T\Delta S + \Delta ZPE$, where ΔZPE is the zero-point energy. The total energy change (ΔE) of these elementary steps are the energy differences between DFT-calculated energies of reactant and product states. Here, for the ORR, we evaluated the binding energies of OH* and O* on the surfaces of the catalysts under consideration. The chemical potential of the solvated proton and electron pair ($H^+ + e^-$) at standard conditions (pH = 0, T = 298.15 K) is calculated as $1/2G_{H2} + eU_{SHE}$ assuming equilibrium at the standard hydrogen electrode. The changes in ΔZPE and $T\Delta S$ are based upon previously determined values.[19] With this approach, the theoretical overpotential of ORR (η^{ORR}) is defined in Equation (4).

$$\eta^{ORR} = 1.23\,V - (G^{ORR}/e)\ V \quad (4)$$

Results and Discussion

Synthesis and Characterization of G6OH($Au_xPd_{(300-x)}$) DENs

The synthetic method used for the preparation of G6OH($Au_xPd_{(300-x)}$) DENs was modified slightly from our previously published reports[4–6] and is provided in the Experimental Section. Briefly, G6OH dendrimers were used as synthetic templates for the synthesis of G6OH($Au_xPd_{(300-x)}$) DENs. It has previously been demonstrated that NPs remain encapsulated within G6OH dendrimers during electrocatalysis,[20] however, for simplicity, we will henceforth refer to G6OH($Au_xPd_{(300-x)}$) DENs simply as $Au_xPd_{(300-x)}$. Therefore, the five catalysts synthesized were Au_{300}, $Au_{250}Pd_{50}$, $Au_{150}Pd_{150}$, $Au_{50}Pd_{250}$, and Pd_{300}. X-ray absorption spectroscopy (XAS) has previously revealed that the AuPd mixed-metal DENs are quasi-random alloys and that the G6OH dendrimer is not coordinated to the surface of the encapsulated nanoparticles.[5]

Representative TEM images for each of these electrocatalysts are provided in Figure S1. Analysis of 200 individual particles yielded the initial size distributions shown in Table 1. The key point is that, within the statistical resolution of the measurements, all five compositions have the same average size with perhaps a slight increase in size as the Pd content increases.

Vulcan carbon and Nafion binder were used to prepare $Au_xPd_{(300-x)}$/C composite inks as discussed in previous reports[21–23] and in the Experimental Section. Scanning transmission electron microscopy (STEM) analysis of the $Au_xPd_{(300-x)}$/Vulcan carbon ($Au_xPd_{(300-x)}$/C) inks revealed no gross size

Table 1. Size distributions of the as-synthesized $Au_xPd_{(300-x)}$ DENs determined by TEM analysis (Figure S1) of 200 randomly selected particles. The two columns on the right of the table are the average ORR onset and peak potentials extracted from ORR CVs like those shown in Figure 5. The onset potential is defined as the potential at 10% of the normalized peak current. Standard deviations are based on three independent experiments.

$Au_xPd_{(300-x)}$	Average size [nm]	Onset potential [V vs. RHE]	Peak potential [V vs. RHE]
Au_{300}	1.6 ± 0.3	0.820 ± 0.002	0.689 ± 0.001
$Au_{250}Pd_{50}$	1.6 ± 0.3	0.841 ± 0.004	0.728 ± 0.004
$Au_{150}Pd_{150}$	1.8 ± 0.4	0.889 ± 0.002	0.790 ± 0.006
$Au_{50}Pd_{250}$	2.0 ± 0.4	0.908 ± 0.003	0.813 ± 0.003
Pd_{300}	2.0 ± 0.4	0.862 ± 0.001	0.737 ± 0.007

changes upon immobilization of the DENs onto the Vulcan carbon support. For example, STEM analysis of $Au_{150}Pd_{150}$ revealed only a slight growth in average particle size from 1.8 ± 0.4 to 2.1 ± 0.6 nm (Figure S2).

Energy dispersive X-ray spectroscopy (EDX) line scans confirmed that the NPs are alloys. For example, Figure 1a is a representative STEM image of a $Au_{150}P_{150}$ NP. The red arrow indicates the line scan analyzed by EDX in Figure 1b. The line scan was conducted on only half of the NP to minimize beam damage during the analysis. The overlap of the atomic profiles suggests alloying of Au (black line) and Pd (red line) for this NP, which is intended to contain 50% of each elements.

Cyclic Voltammetry (CV) Characterization of $Au_xPd_{(300-x)}$/C

Prior to electrochemical characterization, $Au_xPd_{(300-x)}$/C inks were drop-cast onto polished 3 mm-diameter GCEs to form catalyst-modified working electrodes. The $Au_xPd_{(300-x)}$ catalysts were electrochemically cleaned in Ar-saturated, 0.10 M $HClO_4$ (pH = 1.0) by cycling 20 times between 0.05 V and 1.57 V at 200 mV/s, at which point the CVs achieved limiting behavior. Three additional CVs were obtained over the same potential range, and the last of these (Figure 2) was used to characterize the electrocatalyst surfaces.

The CVs in Figure 2 exhibit two main regions of interest: AuO_x reduction peaks at ~1.0 V[3] and PdO_x reduction peaks between 0.5 V and 0.7 V (expanded view in the inset). For

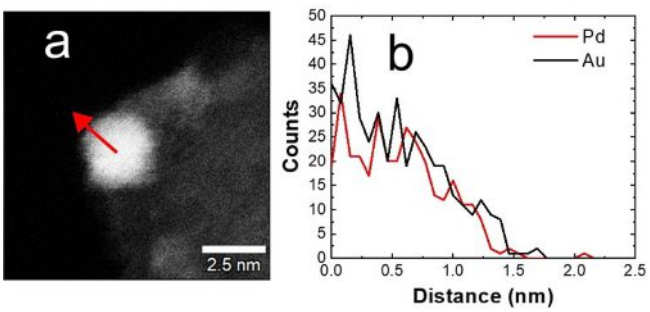

Figure 1. Representative a) aberration-corrected STEM image and b) EDX line scan of $Au_{150}Pd_{150}$. The red arrow on the STEM image correlates to the x-axis of the EDX line scan with the center of the NP corresponding to 0.

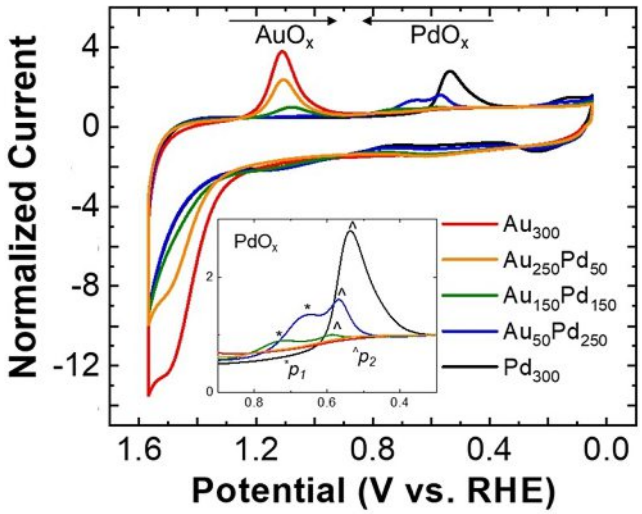

Figure 2. CVs for $Au_xPd_{(300-x)}$ electrocatalysts obtained in Ar-saturated, 0.10 M $HClO_4$. The capacitance of the CVs was normalized at 0.30 V to account for differences in catalyst loading on the electrode surface. The arrows at the top of the figure indicate the direction the peaks move as they become smaller. The inset shows an expanded view of the PdO_x reduction peaks. The two individual PdO_x reduction peaks are indicated with asterisks (*) for p_1 and carrots (^) for p_2, respectively (see text). The $Au_xPd_{(300-x)}$ catalysts were electrochemically cleaned in Ar-saturated, 0.10 M $HClO_4$ (pH = 1.0) by cycling 20 times between 0.05 V and 1.57 V at 200 mV/s. The scan rate for the CVs shown in the figure was 50 mV/s.

$Au_{150}Pd_{150}$, the integrated areas of the AuO_x and PdO_x reduction peaks were converted into relative surface areas, as discussed in the Experimental Section, yielding a calculated surface composition of 51 ± 2% Pd and 49 ± 2% Au. These values provide further evidence that the catalysts are random alloys having surface compositions mirroring the solution compositions used for the synthesis. Unfortunately, integration of the minor Au and Pd peaks of $Au_{50}Pd_{250}$ and $Au_{250}Pd_{50}$, respectively, was complicated by the capacitance of the carbon support, and therefore reliable surface compositions could not be obtained for these materials. Although the electrochemical results discussed here, and the XAS results alluded to earlier,[5] suggest that the surfaces of these DENs are more-or-less random alloys, we cannot rule out the possibility of atomic rearrangements during electrochemical cycling or electrocatalysis as has been observed in other cases.[24]

The AuO_x and PdO_x reduction potentials for all catalysts are provided in Table 2. The $Au_xPd_{(300-x)}$ alloys exhibit surface metal oxide reduction peaks between those observed for Au_{300} and

Table 2. Au- and Pd-oxide reduction peak potentials extracted from the CVs in Figure 2. Standard deviations are based on three independent experiments.

$Au_xPd_{(300-x)}$	AuO_x reduction [V vs. RHE]	PdO_x reduction [V vs. RHE] p_1	p_2
Au_{300}	1.112 ± 0.003	NA	NA
$Au_{250}Pd_{50}$	1.104 ± 0.002	0.765 ± 0.008	NA
$Au_{150}Pd_{150}$	1.078 ± 0.007	0.72 ± 0.01	0.588 ± 0.006
$Au_{50}Pd_{250}$	0.992 ± 0.005	0.633 ± 0.001	0.565 ± 0.001
Pd_{300}	NA	NA	0.544 ± 0.004

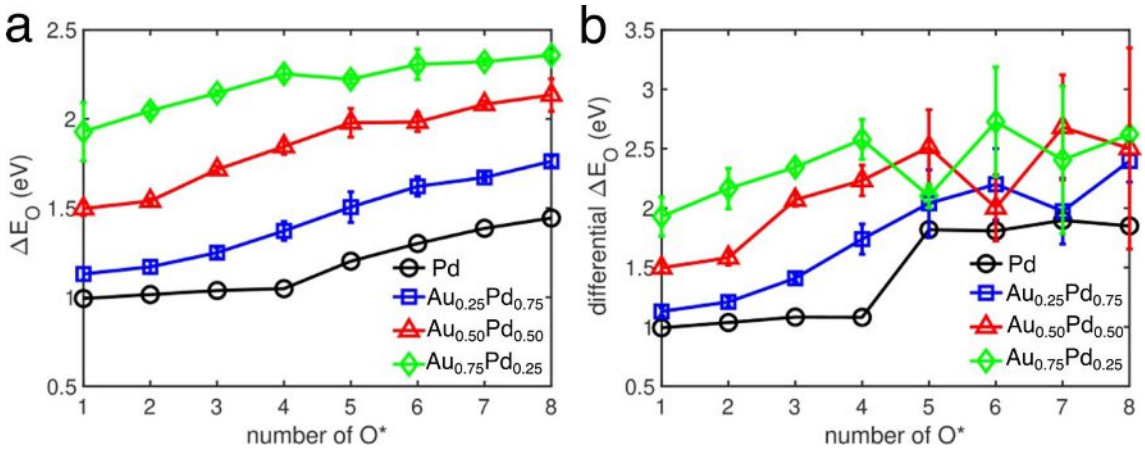

Figure 3. Calculated a) average O binding energy and b) differential O binding energy vs. O coverage for Pd and AuPd alloy surfaces.

Pd_{300}. Specifically, and as indicated by the black arrows toward the top of Figure 2, the AuO_x reduction peak shifts from 1.112 ± 0.003 V for Au_{300} to less positive potentials as the Pd content increases. In contrast, the PdO_x reduction peak for Pd_{300} DENs at 0.544 ± 0.004 V shifts to more positive potentials for the $Au_xPd_{(300-x)}$ alloys.

Importantly, two distinct PdO_x reduction peaks are apparent for the $Au_{150}Pd_{150}$ and for $Au_{50}Pd_{250}$ DENs. The two set of peaks are located around 0.7 V (p_1, marked with asterisks: *, Figure 2 inset) and 0.6 V (p_2, marked with carrots: ^), respectively. In contrast, for $Au_{250}Pd_{50}$ DENs, only a single PdO_x reduction peak at 0.765 V is present. These peaks are all at more positive potentials than the PdO_x reduction peak of Pd_{300} DENs, which indicates that Au alloying facilitates PdO_x reduction. This is likely due to a reduction in the binding strengths of O on AuPd alloy surfaces. Similar behavior has been reported for bulk-phase surface alloys of Au and Pd.[9]

Theoretical calculations were employed to further understand the shift in the PdO_x reduction peaks of the AuPd alloy surfaces. To this end, the average O binding energy (ΔE_O) and differential O binding energy were calculated as a function of O coverage and Pd composition, as shown in Figure 3. The optimized surface structures are shown in Figure S3 (for the alloy surfaces, only one out of the three random alloy distributions is shown). Figure 3 shows that the average O binding energy increases with increasing O coverage, which is due to adsorbate-adsorbate repulsion. Independent of O coverage, Au alloying significantly weakens the O binding compared to the Pd-only surface. The weakening of O adsorption can be primarily attributed to the electronic (or ligand) effect between Au and Pd, at least for $Au_{0.25}Pd_{0.75}$ and $Au_{0.50}Pd_{0.50}$ compositions at low O coverages. The reason for this is that at low coverage, O atoms only bind to Pd_3 hollow sites (as on the Pd-only surface), because the binding energies on the alloy surfaces are significantly weaker. O adsorption at mixed-metal sites (Au_1Pd_2 and Au_2Pd_1), for which the energy is primarily determined by ensemble effects, only occurs at high O coverages on the $Au_{0.25}Pd_{0.75}$ and $Au_{0.50}Pd_{0.50}$ alloys or at low Pd composition (i.e., $Au_{0.75}Pd_{0.25}$).

Surface phase diagrams (Figure 4), which depict the stable surface states as a function of applied potential, were constructed based on the calculated O binding energies. For pure Pd, the clean surface and 4O-covered surface (1/4 ML O) is bi-stable at an applied potential of 0.55 V. This is consistent with the experimentally observed PdO_x reduction peak of Pd_{300} DENs at 0.544 V. The 4O-covered surface remains the most stable surface for a wide potential window from 0.55 V to 0.90 V, at which point the 6O surface (3/8 ML O) takes over. For $Au_{0.25}Pd_{0.75}$, the 2O and 3O surfaces are stable at ~0.60 V and ~0.70 V, respectively. These computational results qualitatively explain the two distinct PdO_x reduction potentials in the $Au_{50}Pd_{250}$ DENs located at 0.565 and 0.633 V.

For the $Au_{0.50}Pd_{0.50}$ alloy model, O atoms start to bind at ~0.80 V. The splitting of the experimental PdO_x peaks in the

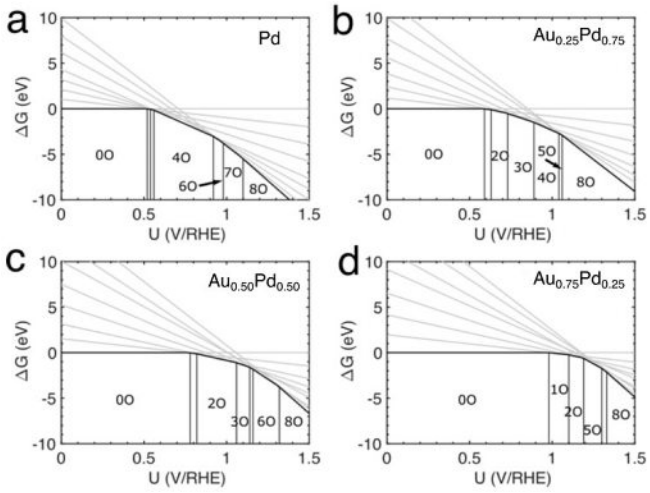

Figure 4. Surface phase diagram for Pd and AuPd alloy surfaces. a) Pd, b) $Au_{0.25}Pd_{0.75}$, c) $Au_{0.50}Pd_{0.50}$, d) $Au_{0.75}Pd_{0.25}$. The stable surface phases at different applied potentials correspond to the lowest free energy of formation. The gray lines show the free energies of formation of various surface phases that are not stable under different potentials. The free energies of stable phases are denoted by black lines. The stable surface phases are annotated.

CVs of the $Au_{50}Pd_{250}$ and $Au_{150}Pd_{150}$ catalysts is therefore likely a consequence of increased O–O repulsion on the alloy surfaces. This repulsion is a result of the decreased Pd surface area, wherein adsorbed O atoms on the Pd domains are forced to be closer together. For the $Au_{0.75}Pd_{0.25}$ model, the surface is free of oxygen adsorbates below 1.0 V. Obviously, more Au alloying increases the PdO_x reduction potential as a result of weaker O binding energies. The low PdO_x reduction potential at ~0.50 V (p_2 peaks in Figure 2) is not observed for the $Au_{150}Pd_{150}$ and $Au_{250}Pd_{50}$ catalysts. This inconsistency may be due to the existence of Pd-rich patches on the surface of the DENs, which are not present in our random alloy models.

The foregoing results are significant because PdO_x reduction potentials have previously been reported to be related to the O-binding energy of Pd-based catalysts.[2,3] For example, when Pd surfaces bind oxygen strongly, it is difficult to reduce PdO_x and therefore the corresponding reduction peak will shift to less positive potentials. Pd-only catalysts typically bind oxygen too strongly for optimal oxygen reduction electrocatalysis, and this limits their effectiveness for the ORR. Accordingly, in the next section, the PdO_x reduction potentials for $Au_xPd_{(300-x)}$ DENs will be correlated to ORR activity.

Electrocatalytic ORR activity of $Au_xPd_{(300-x)}$/C

Following electrochemical cleaning and surface characterization, the ORR activity of the $Au_xPd_{(300-x)}$ electrocatalysts was analyzed in O_2-saturated, 0.10 KOH. Figure 5 shows representative ORR CVs for each electrocatalyst. The average ORR current onset potentials (defined as the potential corresponding to 10% of the normalized peak current) and peak potentials are provided in Table 1. The trend in ORR activity can be correlated to the O-binding energies of the catalysts, which are an important descriptor of ORR activity.[6,8,25] For example, it has previously been reported that Au is a poor ORR catalyst due to its weak O-binding energy relative to Pt and Pd.[2] Consistent with this finding, Pd_{300} in our study has an onset potential ~42 mV more positive than Au_{300}. Pd, however, is typically a less active ORR catalyst compared to Pt due to the fact that Pd binds oxygen too strongly.[3]

Alloying of strong and weak O-binding metals has previously been shown to be an effective means for tuning the ORR activity of electrocatalysts.[8,19] Indeed, we observe this effect in the $Au_xPd_{(300-x)}$ alloys. For example, the onset potential for the ORR electrocatalyzed by $Au_{250}Pd_{50}$ increases by ~21 mV relative to Au_{300} (Table 1). $Au_xPd_{(300-x)}$ alloys containing ≥50% Pd lead to ORR onset potentials that exceed that of Pd_{300}. Specifically, the $Au_{150}Pd_{150}$ and $Au_{50}Pd_{250}$ electrocatalysts have onset potentials positive of Pd_{300} by ~27 mV and ~46 mV. This increase in ORR activity is consistent with the reduced O-binding energies of these catalysts as discussed in the previous section. Interestingly, however, while the PdO_x reduction potentials trend more-or-less linearly with Pd-composition (Figure 6), the corresponding ORR peak potentials exhibit a volcano-shaped dependence. This is significant because it indicates that while decreasing the O-binding energy relative to pure Pd increases the ORR activity, there is an optimal O-binding energy for optimal performance.

So far, we have only discussed the effect of O-binding energies of Pd-based active sites for the ORR. However, it is also important to consider the relative effect of the O-binding energies of the Au-surface sites on ORR activity. For example, the negative shift in the AuO_x reduction potential with increasing Pd-content indicates that these alloyed surface sites bind oxygen more strongly than Au_{300}, thereby increasing the relative ORR activity of Au-based active sites. Despite this observation, and because Au NPs are significantly less active for the ORR than Pd NPs, we conclude that the increased O-binding energy of the Au-based active sites is not as influential on overall ORR activity as Pd active sites. To better understand this observation, we have conducted calculations of the ORR activity on PdAu alloy catalysts.

We first consider the ORR activities of Pd(111) surfaces having different degrees of oxidation using the computational hydrogen electrode method.[19] Free energy diagrams for the ORR on different Pd surfaces are shown in Figure S4. For clean Pd(111), the ORR onset potential is ~0.3 V, which is low due to

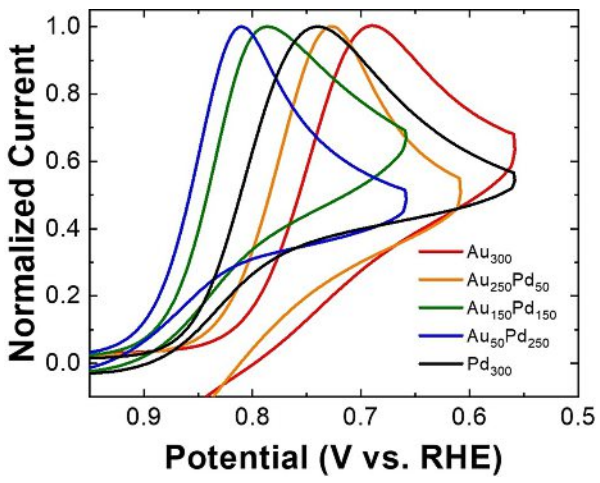

Figure 5. CVs of $Au_xPd_{(300-x)}$ electrocatalysts obtained in O_2-saturated, 0.10 M KOH. The CVs were normalized to account for small differences in mass-loading of the catalyst. The scan rate was 20 mV/s.

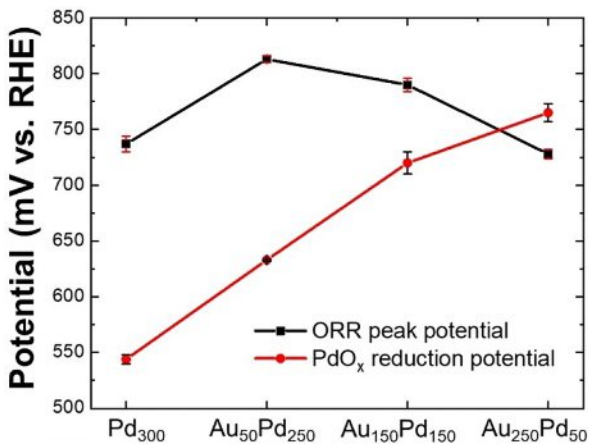

Figure 6. Plots of the ORR peak potential and PdO_x reduction potential as a function of electrocatalyst composition. For the catalysts having more than one PdO_x reduction potential (i.e., $Au_{50}Pd_{250}$ and $Au_{150}Pd_{150}$, Table 2), the most positive reduction potential, p_1, was used. Standard deviations are based on three independent experiments.

overly strong O adsorption. On a 1/4 ML O-covered Pd surface, the onset potential of the ORR increases dramatically to 0.84 V. This is because adsorbate-adsorbate repulsion greatly destabilizes O adsorption. Accordingly, the potential-limiting process switches from O* reduction on the clean Pd surface to OH* reduction. Theoretically, ORR activity can be further improved by further destabilizing O* and OH*. Increasing the O coverage to 3/8 ML, however, makes OH adsorption too weak relative to the O binding strength, and this leads to a decreased ORR onset potential of 0.58 V. Thus, we find that the 1/4 ML O-covered Pd (111) surface is the most active for the ORR. Moreover, the active site is between two O* adsorbed at the 3-fold hollow site. The details of the adsorption configurations at the active site is shown in Figure S5.

We anticipated that by alloying Pd with Au, the adsorption energy of O* and OH* would be more properly tuned to further enhance the ORR activity of Pd. To determine if there is such an active site on AuPd surfaces, we refer to the differential O adsorption energy shown in Figure 3b. It describes the adsorption energy of each subsequently deposited O on the surface. For a pure Pd surface, the O binding energy remains roughly constant at 1 eV up to an O coverage of 1/4 ML. Upon adsorption of the fifth O, however, the O adsorption energy jumps to 1.8 eV and then remains fairly constant up to an O coverage of 1/2 ML. Our goal, therefore, is to search for the right composition and O* coverage on AuPd surfaces to obtain an O binding energy above 1.8 eV. For $Au_{0.25}Pd_{0.75}$, the fifth O has a binding energy of about 2 eV, which matches our target. Using the same criteria, we can see that $3O/Au_{0.50}Pd_{0.50}$ and $1O/Au_{0.75}Pd_{0.25}$ surfaces also have O binding energies similar to 2 eV.

On the basis of our O binding energy calculations, we have thus far identified three alloy surfaces that are potentially more active for the ORR than the Pd-only surface: $5O/Au_{0.25}Pd_{0.75}$, $3O/Au_{0.50}Pd_{0.50}$, and $1O/Au_{0.75}Pd_{0.25}$. However, a suitable OH binding energy is also required to yield enhanced ORR activity. Accordingly, we then explicitly examined the ORR activities of alloy surfaces using the computational hydrogen electrode method.[19]

The ORR activities of selected random AuPd alloy surfaces are shown in Figure 7. For the specific $Pd_{0.75}Au_{0.25}$ surface shown in Figure 7a, the ORR onset potential is 0.95 V, which is higher than the 1/4 ML O-covered Pd surface. The O binding energy at this site is 1.9 eV, which is a little higher than that of the Pd surface (1.8 eV). The mild destabilization of O* is caused by electronic effects arising from the Au component. Similarly, the OH* binding energy is also increased by 0.12 eV. For the $Au_{0.50}Pd_{0.50}$ and $Au_{0.75}Pd_{0.25}$ surfaces, the O binding energies are also about 1.9 eV. The OH binding energies on $Au_{0.50}Pd_{0.50}$ and $Au_{0.75}Pd_{0.25}$ surfaces are weaker than those on $Au_{0.25}Pd_{0.75}$ due to

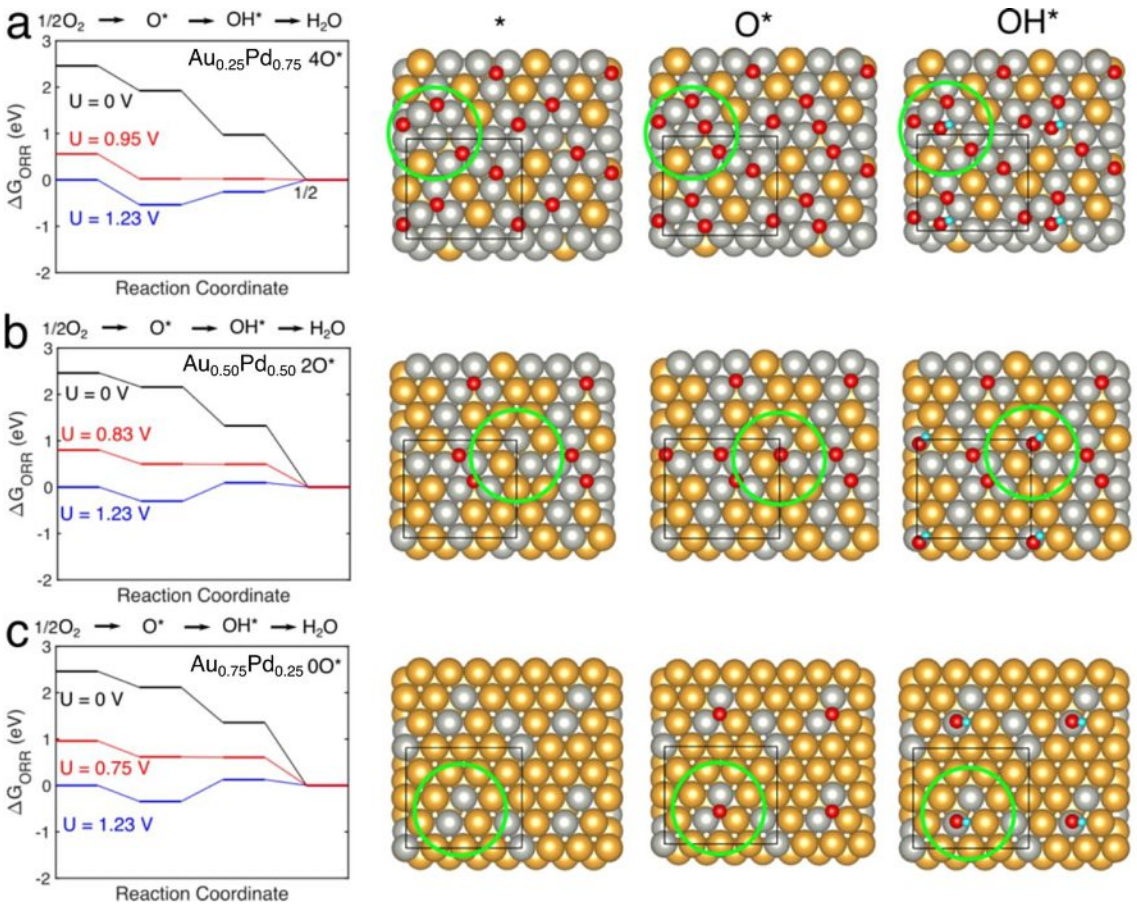

Figure 7. Free energy diagrams for the ORR on $Au_{0.25}Pd_{0.75}$, $Au_{0.50}Pd_{0.50}$, $Au_{0.75}Pd_{0.25}$. The atomic structures of the active sites are shown to the right of the free energy diagrams.

the higher Au content. The over-destabilization of OH* reduces the ORR onset potentials to 0.83 V and 0.75 V for $Au_{0.50}Pd_{0.50}$ and $Au_{0.75}Pd_{0.25}$, respectively. The active site for the ORR on the $Au_{0.50}Pd_{0.50}$ and $Au_{0.75}Pd_{0.25}$ surfaces also changes to a $AuPd_2$ site due to the diminished Pd surface content. It should be noted that the random alloys have various local Au/Pd distributions that can cause different ORR activities. Specifically, we observe fluctuations of ORR activity in our calculations due to local surface structures, which will be the focus of a future study.

2. Summary and Conclusions

We synthesized five different compositions of $Au_xPd_{(300-x)}$ DENs and analyzed their ORR activity in 0.10 M KOH using cyclic voltammetry. While Pd is active for the ORR in alkaline media, Pd-only catalysts typically bind oxygen too strongly. Alloying Pd with Au, which weakly binds oxygen, weakens the O-binding energy on $Au_xPd_{(300-x)}$ alloys, thereby enhancing ORR activity. The relative O-binding energies of Pd-containing surface ensembles were experimentally correlated to the PdO_x reduction potentials observed during cyclic voltammetry in 0.10 M $HClO_4$. Significantly, a linear trend in PdO_x reduction potentials with Pd-composition correlated to a non-linear trend in ORR peak potentials. Specifically, a ~89 mV shift in PdO_x reduction potential for $Au_{50}Pd_{250}$, relative to Pd_{300}, resulted in a maximum ORR peak potential of 0.813 ± 0.002 V.

The findings reported here are important because they reveal the possibility of correlating redox potentials to the O-binding energies of particular active sites on the surface of nanoalloys. The modulation of adsorbate binding strength with catalyst composition is a vital concept in theoretical predictions of electrocatalyst activities. The theoretical findings presented here indicate that alloying Pd with Au weakens the O binding energy. Pd catalysts with 25 at% Au have weaker O and OH binding energies as compared to pure Pd catalysts, leading to enhanced ORR activity. A further increase in the Au composition results in decreased ORR activity due to a weakened OH binding energy.

Acknowledgements

We gratefully acknowledge support from the Chemical Sciences, Geosciences, and Biosciences Division, Office of Basic Energy Sciences, Office of Science, U.S. Department of Energy (Contract: DE-SC0010576). We thank the Robert A. Welch Foundation RMC: Grant (F-0032 and GH: Grant F-1841) for sustained support of our research. Computational resources were provided by the National Energy Research Scientific Computing Center and the Texas Advanced Computing Center. We thank Dr. Karalee Jarvis (Texas Materials Institute) for assistance with the electron microscopy.

Conflict of Interest

The authors declare no conflict of interest.

Keywords: alloys · electrocatalysis · nanoalloys · oxygen reduction reaction · density functional theory

[1] H. Li, L. Luo, P. Kunal, C. S. S. Bonifacio, Z. Duan, J. C. C. Yang, S. M. Humphrey, R. M. Crooks, G. Henkelman, *J. Phys. Chem. C* **2018**, *122*, 2712–2716.
[2] X. Huang, A. J. Shumski, X. Zhang, C. W. Li, *J. Am. Chem. Soc.* **2018**, *140*, 8918–8923.
[3] G. Wang, J. Guan, L. Xiao, B. Huang, N. Wu, J. Lu, L. Zhuang, *Nano Energy* **2016**, *29*, 268–274.
[4] M. G. Weir, M. R. Knecht, A. I. Frenkel, R. M. Crooks, *Langmuir* **2010**, *26*, 1137–1146.
[5] M. R. Knecht, M. G. Weir, A. I. Frenkel, R. M. Crooks, *Chem. Mater.* **2008**, *20*, 1019–1028.
[6] L. Luo, L. Zhang, G. Henkelman, R. M. Crooks, *J. Phys. Chem. Lett.* **2015**, *6*, 2562–2568.
[7] L. Zhang, R. M. Anderson, R. M. Crooks, G. Henkelman, *Surf. Sci.* **2015**, *640*, 65–72.
[8] L. Luo, Z. Duan, H. Li, J. Kim, G. Henkelman, R. M. Crooks, *J. Am. Chem. Soc.* **2017**, *139*, 5538–5546.
[9] H. Erikson, M. Liik, A. Sarapuu, M. Marandi, V. V. Sammelselg, K. Tammeveski, *J. Electroanal. Chem.* **2013**, *691*, 35–41.
[10] D. F. Yancey, E. V. Carino, R. M. Crooks, *J. Am. Chem. Soc.* **2010**, *132*, 10988–10989.
[11] G. Kresse, J. Hafner, *Phys. Rev. B* **1993**, *47*, 558–561.
[12] G. Kresse, J. Furthmüller, *Comput. Mater. Sci.* **1996**, *6*, 15–50.
[13] G. Kresse, J. Furthmüller, *Phys. Rev. B* **1996**, *54*, 11169–11186.
[14] J. P. Perdew, K. Burke, M. Ernzerhof, *Phys. Rev. Lett.* **1996**, *77*, 3865–3868.
[15] P. E. Blöchl, *Phys. Rev. B* **1994**, *50*, 17953–17979.
[16] H. Monkhorst, J. Pack, *Phys. Rev. B* **1976**, *13*, 5188–5192.
[17] C. D. Taylor, S. A. Wasileski, J. S. Filhol, M. Neurock, *Phys. Rev. B* **2006**, *73*, 165402.
[18] K. Mathew, R. Sundararaman, K. Letchworth-Weaver, T. A. Arias, R. G. Hennig, *J. Chem. Phys.* **2014**, *140*, DOI 10.1063/1.4865107.
[19] J. K. Nørskov, J. Rossmeisl, A. Logadottir, L. Lindqvist, J. R. Kitchin, T. Bligaard, H. Jónsson, *J. Phys. Chem. B* **2004**, *108*, 17886–17892.
[20] C. L. Jackson, H. D. Chanzy, F. P. Booy, B. J. Drake, D. A. Tomalia, B. J. Bauer, E. J. Amis, *Macromolecules* **1998**, *31*, 6259–6265.
[21] E. Andrews, S. Katla, C. Kumar, M. Patterson, P. Sprunger, J. C. Flake, *J. Electrochem. Soc.* **2015**, *162*, F1373–F1378.
[22] E. Andrews, J. C. Flake, Y. Fang, *ECS Trans.* **2014**, *66*, 67–70.
[23] D. R. Kauffman, D. Alfonso, C. Matranga, H. Qian, R. Jin, *J. Am. Chem. Soc.* **2012**, *134*, 10237–10243.
[24] V. Petrykin, J. E. Mueller, D. Fantauzzi, P. Krtil, *ChemElectroChem* **2014**, *1*, 207–212.
[25] L. Zhang, G. Henkelman, *J. Phys. Chem. C* **2012**, *116*, 20860–20865.

Manuscript received: July 23, 2020
Revised manuscript received: August 17, 2020